Inorg. Chem. **2008**, *47*, 11405−11416

Synthesis, Characterization, and Thermal Properties of Homoleptic Rare-Earth Guanidinates: Promising Precursors for MOCVD and ALD of Rare-Earth Oxide Thin Films

Andrian P. Milanov, Roland A. Fischer, and Anjana Devi*

Inorganic Materials Chemistry Group, Lehrstuhl für Anorganische Chemie II, Ruhr-University Bochum, D-44780, Bochum, Germany

Received July 30, 2008

Eight novel homoleptic tris-guanidinato complexes $M[(N^iPr)_2CNR_2]_3$ [M = Y (**a**), Gd (**b**), Dy (**c**) and R = Me (**1**), Et (**2**), ^{i}Pr (**3**)] have been synthesized and characterized by NMR, CHN-analysis, mass spectrometry and infrared spectroscopy. Single crystal structure analysis revealed that all the compounds are monomers with the rare-earth metal center coordinated to six nitrogen atoms of the three chelating guanidinato ligands in a distorted trigonal prism geometry. With the use of TGA/DTA and isothermal TGA analysis, the thermal characteristics of all the complexes were studied in detail to evaluate their suitability as precursors for thin film deposition by MOCVD and ALD. The ^{i}Pr-Me_2N-guanidinates of Y, Gd and Dy (**1a**−**c**) showed excellent thermal characteristics in terms of thermal stability and volatility. Additionally, the thermal stability of the ^{i}Pr-Me_2N-guanidinates of Y and Dy (**1a**, **c**) in solution was investigated by carrying out NMR decomposition experiments and both the compounds were found to be remarkably stable. All these studies indicate that ^{i}Pr-Me_2N-guanidinates of Y, Gd and Dy (**1a**−**c**) have the prerequisites for MOCVD and ALD applications which were confirmed by the successful deposition of Gd_2O_3 and Dy_2O_3 thin films on Si(100) substrates. The MOCVD grown films of Gd_2O_3 and Dy_2O_3 were highly oriented in the cubic phase, while the ALD grown films were amorphous.

Introduction

Rare-earth oxide thin films are emerging materials for applications in many different fields of technology. Because of their high thermal stability, they are of interest as wear- and corrosion-resistant coatings.[1−3] High refractive indices (1.91−1.98) of the rare-earth oxide films make them applicable in optics, for example, as antireflection coatings.[4] Their high dielectric constants (e.g., $k(La_2O_3) = 27$, $k(Gd_2O_3) = 16$, $k(Dy_2O_3) = 14-18$), large band gaps ($E_g(Gd_2O_3) = 5.6$ eV, $E_g(Dy_2O_3) = 4.9$ eV) and high thermodynamic stability on silicon (higher than for ZrO_2 and HfO_2) classify these materials for high-k applications.[5] In addition, rare-earth oxides are also components of superconducting oxide phases[6] and thermoelectric oxides,[7,8] and in particular, Gd_2O_3 is being investigated as a promising passivation layer for GaAs.[9] These potential applications have enhanced the research activities related to the growth of high quality thin films of rare-earth oxides by several techniques, which include physical vapor deposition (PVD) methods, such as sputtering, molecular beam epitaxy (MBE), and chemical methods such as metalorganic chemical vapor deposition (MOCVD) and atomic layer deposition (ALD). Thin film growth of rare-earth oxides by MOCVD and ALD have received increased attention in recent years as they offer the potential for large area deposition, good composition control

* To whom correspondence should be addressed. E-mail: anjana.devi@rub.de.

(1) Bonnet, G.; Lachkar, M.; Larpin, J. P.; Colson, J. C. *Solid State Ionics* **1994**, *72*, 344.
(2) Bonnet, G.; Lachkar, M.; Colson, J. C.; Larpin, J. P. *Thin Solid Films* **1995**, *261*, 31.
(3) Sigler, D. R. *Oxid. Met.* **1993**, *40*, 295.
(4) Heitmann, W. *Appl. Opt.* **1973**, *12*, 394.
(5) (a) Wilk, G. D.; Wallace, R. M.; Anthony, J. M. *J. Appl. Phys.* **2001**, *89*, 5243. (b) Leskelä, M; Ritala, M. *J. Solid State Chem.* **2003**, *171*, 170. (c) Päiväsaari, J.; Putkonen, M.; Niinistö, L. *Thin Solid Films* **2005**, *472*, 275 and references therein.
(6) MacManus-Driscoll, J. L. *Annu. Rev. Mater. Sci.* **1998**, *28* 421 and references therein.
(7) Scullin, M. L.; Yu, C.; Huijben, M.; Mukerjee, S.; Seidel, J.; Zhan, Q.; Moore, J.; Majumdar, A.; Ramesh, R. *Appl. Phys. Lett.* **2008**, *92*, 202113.
(8) Weidenkaff, A.; Robert, R.; Aguirre, M.; Bocher, L.; Lippert, T.; Canulescu, S. *Renewable Energy* **2008**, *33* (2), 342.
(9) Hong, M.; Kwo, J.; Kortan, A. R.; Mannearts, J. P.; Sergent, A. M. *Science* **1999**, *283*, 1897.

10.1021/ic801432b CCC: $40.75
Published on Web 11/07/2008

Scheme 1. Resonance Structures of the Guanidinate Ligand

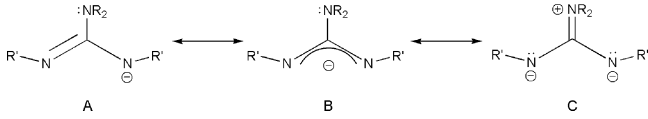

and film uniformity as well as excellent conformal coverage on nonplanar device geometries. Nowadays, these issues are very crucial, as size of the device structures are shrinking and getting more complex especially for microelectronic and nanoelectronic applications.[10] In general, there are fewer reports on MOCVD/ALD growth compared to the PVD grown rare-earth oxides. This is basically due to the lack of suitable precursors with appropriate volatility, stability and decomposition characteristics for MOCVD and ALD processes. Since the rare-earth halides are not sufficiently volatile, MOCVD and ALD precursors have been chosen from a small range of volatile metal-organic rare earth compounds which includes mainly homoleptic precursors containing β-diketonate,[7,11−18] cyclopentadienyl,[19,20] bis(trimethylsilyl)amido[21−24] and amidinato ligands.[25−28] Among them, the amidinates have shown promising thermal properties with [La(^{i}PrAMD)$_3$] being one of the most volatile rare-earth compounds reported by Lim et al.[25]

Recent reports have shown that the related *N*,*N*′-dialkyl-2-dialkylamido-guanidinate anion [(R′N)$_2$CNR$_2$]$^-$ can impart a similar coordination environment as an amidinate anion while offering increased stability due to the possibility of the additional zwitterionic resonance structure **C** shown in Scheme 1.[29] Moreover, the guanidinate ligand provides tuneability in terms of steric and electronic properties, by

Scheme 2. Synthesis of the Homoleptic Rare Earth Guanidinates

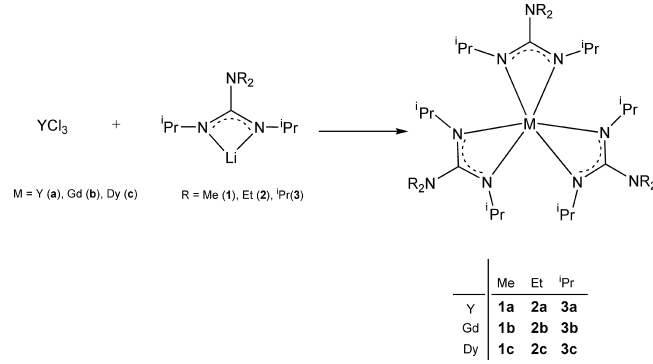

	Me	Et	^{i}Pr
Y	**1a**	**2a**	**3a**
Gd	**1b**	**2b**	**3b**
Dy	**1c**	**2c**	**3c**

variation of the substituents R and R′. Consequently, an increase in the volatility of guanidinate compounds of the large rare earth metals is expected. In addition, the bidentate chelating effect of the guanidinate ligands is expected to enhance the thermal/chemical stability of the resulting metal complexes and thus make them suitable precursors for MOCVD and ALD. Furthermore, it has been proposed that donation of the lone pair from the dialkylamido into the π-system of the ligand could result in metal complexes being electron rich when compared to other ligands, such as amidinates.[30]

In our previous work, we reported guanidinate complexes of group IV transition metals that showed promising properties as precursors for vapor deposition techniques.[31,32] With these precursors, we were able to grow high quality oxide thin films applying different deposition techniques (MOCVD, liquid injection MOCVD and ALD).[32−34] In this work, we adopted a similar approach in terms of ligand engineering for rare-earth elements and our primary goal was to synthesize homoleptic rare-earth guanidinate complexes, and study their structure and reactivity in order to evaluate them as precursors for MOCVD and ALD of rare-earth oxide films. To date, some monoguanidinate,[35,36] bis-guanidinate,[37−41] and very few homoleptic tris-guanidinate rare-earth complexes have been reported in the literature.[42−45] For all these com-

(10) The International Technology Roadmap for Semiconductors, Semiconductor Industry Association, 2007. http://public.itrs.net.
(11) Päiväsaari, J.; Putkonen, M.; Sajavaara, T.; Niinistö, L. *J. Alloys Compd.* **2004**, *374*, 124.
(12) Puurunen, R. L. *Chem. Vap. Deposition* **2003**, *9*, 327.
(13) Bernay, C.; Ringuedé, A.; Colomban, P.; Lincot, D.; Cassir, M. *J. Phys. Chem. Solids* **2003**, *64*, 1761.
(14) Deacon, G. B.; MacKinnon, P.; Dickson, R. S.; Pain, G. N.; West, B. O. *Appl. Organomet. Chem.* **1990**, *4*, 439.
(15) Milt, V. G.; Ulla, M. A.; Lombardo, E. A. *J. Catal.* **2001**, *200*, 241.
(16) Van, T. T.; Chang, J. P. *Appl. Surf. Sci.* **2005**, *246*, 250.
(17) Putkonen, M.; Nieminen, M.; Niinistö, J.; Niinistö, L.; Sajavaara, T. *Chem. Mater.* **2001**, *12*, 4701.
(18) Putkonen, M; Sajavaara, T.; Johansson, L.-S.; Niinistö, L. *Chem. Vap. Deposition* **2001**, *7*, 44.
(19) Scarel, G.; Bonera, E.; Wiemer, C.; Tallarida, G.; Spiga, S.; Fanciulli, M.; Fedushkin, I. L.; Schumann, H.; Lebedinskii, Y.; Zenkevich, A. *Appl. Phys. Lett.* **2004**, *85*, 630.
(20) Niinistö, J.; Putkonen, M.; Niinistä, L. *Chem. Mater.* **2004**, *16*, 2953.
(21) Triyoso, D. H.; Hegde, R. I.; Grant, J. M.; Schaeffer, J. K.; Roan, D.; White, B. E., Jr.; Tobin, P. J. *J. Vac. Sci. Technol.* **2005**, *B23*, 288.
(22) Kukli, K.; Ritala, M.; Pore, V.; Leskelä, M.; Sajavaara, T.; Hegde, R. I.; Gilmer, D. C.; Tobin, P. J.; Jones, A. C.; Aspinall, H. C. *Chem. Vap. Deposition* **2006**, *12*, 158.
(23) Kukli, K.; Ritala, M.; Pilvi, T.; Sajavaara, T.; Leskelä, M.; Jones, A. C.; Aspinall, H. C.; Gilmer, D. C.; Tobin, P. J. *Chem. Mater.* **2004**, *16*, 5162.
(24) Jones, A. C.; Aspinall, H. C.; Chalker, P. R.; Potter, R. J.; Kukli, K.; Rahtu, A.; Ritala, M.; Leskelä, M. *J. Mater. Chem.* **2004**, *14*, 3101.
(25) Lim, B. S.; Rahtu, A.; De Rouffignac, P.; Gordon, R. G. *Appl. Phys. Lett.* **2004**, *84*, 3957.
(26) Lim, B. S.; Rahtu, A.; Gordon, R. G. *Nat. Mater.* **2003**, *2*, 749.
(27) Lim, B. S.; Rahtu, A.; Park, J.-S.; Gordon, R. G. *Inorg. Chem.* **2003**, *42*, 7951.
(28) Kim, H. K.; Farmer, D. B.; Lehn, J.-S. M.; Rao, P. V.; Gordon, R. G. *Appl. Phys. Lett.* **2006**, *89*, 133512.
(29) Bailey, P. J.; Pace, S. *Coord. Chem. Rev.* **2001**, *214*, 91.
(30) Mullins, S. M.; Duncan, A. P.; Bergman, R. G.; Arnold, J. *Inorg. Chem.* **2001**, *40*, 6952.
(31) Devi, A.; Bhakta, R.; Milanov, A.; Hellwig, M.; Barreca, D.; Tondello, E.; Thomas, R.; Ehrhart, P.; Winter, M.; Fischer, R. A. *Dalton Trans.* **2007**, 1671.
(32) Milanov, A.; Bhakta, R.; Baunemann, A.; Becker, H.-W.; Thomas, R.; Ehrhart, P.; Winter, M.; Devi, A. *Inorg. Chem.* **2006**, *45*, 11008.
(33) Thomas, R.; Rije, E.; Ehrhart, P.; Milanov, A.; Bhakta, R.; Baunemann, A.; Devi, A.; Rischer, R. A.; Waser, R *J. Electrochem. Soc.* **2007**, *154*, G77.
(34) Milanov, A.; Parala, H.; Fischer, R. A.; Devi, A., unpublished results.
(35) Giesbrecht, G. R.; Whitener, G. D.; Arnold, J. *J. Chem. Soc., Dalton Trans.* **2001**, 923.
(36) Yuan, F; Zhu, Y.; Xiong, L. *J. Organomet. Chem.* **2006**, *691*, 3377.
(37) Zhou, Y; Yapp, G. P. A.; Richeson, D. S. *Organometallics* **1998**, *17*, 4387.
(38) Lu, Z.; Yapp, G. P. A.; Richeson, D. S. *Organometallics* **2001**, *20*, 706.
(39) Luo, Y.; Yao, Y.; Shen, Q.; Yu, K.; Weng, L. *Eur. J. Inorg. Chem.* **2003**, 318.
(40) Trifonov, A. A.; Fedorova, E. A.; Fukin, G. K.; Bochkarev, M. N. *Eur. J. Inorg. Chem.* **2004**, 4396.
(41) Trifonov, A. A.; Skvortsov, G. G.; Lyubov, D. M.; Skorodumova, N. A.; Fukin, G. K.; Baranov, E. V.; Glushakova, V. N. *Chem.−Eur. J.* **2006**, *12*, 5320.

Table 1. Crystal Data and Details of Structure Determination for **1a**−**c**, **2a**−**c** and **3b**,**c**

	1a	**1b**	**1c**	**2a**	**2b**	**2c**	**3b**	**3c**
formula	$C_{27}H_{60}N_9Y$	$C_{27}H_{60}N_9Gd$	$C_{27}H_{60}N_9Dy$	$C_{39}H_{84}N_9Y$	$C_{39}H_{84}N_9Gd$	$C_{39}H_{84}N_9Dy$	$C_{45}H_{96}N_9Gd$	$C_{45}H_{96}N_9Dy$
M_r (g•mol^{-1})	599.75	668.09	673.34	768.06	836.39	839.64	920.56	923.79
temperature (K)	113(2)	113(2)	113(2)	113(2)	113(2)	113(2)	113(2)	113(2)
wavelength (Å)	0.71073	0.71073	0.71073	0.71073	0.71073	0.71073	0.71073	0.71073
crystal system	triclinic	triclinic	triclinic	monoclinic	monoclinic	monoclinic	monoclinic	monoclinic
space group	$P\bar{1}$	$P\bar{1}$	$P\bar{1}$	$C2/c$	$C2/c$	$C2/c$	$C2/c$	$C2/c$
a (Å)	10.7165(5)	10.7314(2)	10.7312(3)	22.310(10)	22.2187(14)	22.1555(12)	23.0567(13)	23.061(4)
b (Å)	11.1694(6)	11.2394(2)	11.2048(3)	13.165(3)	13.1014(5)	13.1098(4)	13.2892(6)	13.3482(10)
c (Å)	16.1278(6)	16.0701(3)	16.1286(5)	17.466(5)	17.3788(8)	17.3510(7)	19.4508(9)	19.5859(18)
α (deg)	91.657(4)	91.602(2)	91.639(2)	90	90	90	90	90
β (deg)	95.859(4)	95.622(2)	95.779(2)	114.43(3)	114.313(6)	114.215(5)	118.558(5)	118.741(8)
γ (deg)	115.249(5)	115.210(2)	115.322(3)	90	90	90	90	90
volume (Å^3)	1731.25(14)	1740.00(6)	1738.53(9)	4671(3)	4611.2(4)	4596.2(2)	5234.7(4)	5268.2(11)
Z	2	2	2	4	4	4	4	4
$D_{calc.}$ (g•cm^{-3})	1.151	1.275	1.286	1.092	1.084	1.213	1.168	1.161
μ (mm^{-1})	1.713	1.934	2.177	1.283	1.466	1.660	1.303	1.449
F(000)	648	698	702	1680	1588	1780	1972	1972
crystal size (mm)	0.27 × 0.24 × 0.16	0.38 × 0.30 × 0.25	0.25 × 0.22 × 0.20	0.35 × 0.28 × 0.25	0.28 × 0.25 × 0.15	0.30 × 0.25 × 0.20	0.35 × 0.30 × 0.20	0.340.33 × 0.30
θ range (deg)	3.12−25.00	3.11−25.00	2.60−25.00	2.80−25.00	2.81−25.00	2.82−25.00	3.07−25.00	2.58−25.00
reflns collected	22752	28558	13788	18998	35372	18529	21309	21324
unique reflns	6062 (R_{int} = 0.0686)	6104 (R_{int} = 0.0347)	6092 (R_{int} = 0.0686)	4107 (R_{int} = 0.1121)	4062 (R_{int} = 0.0686)	4045 (R_{int} = 0.0484)	4594 (R_{int} = 0.0395)	4637 (R_{int} = 0.0387)
completeness to θ (θ = 25)	99.7%	99.8%	99.6%	99.8%	99.9%	99.7%	99.7%	99.7%
data/ restraints/parameters	6062/0/334	6104/0/334	6092/0/334	4107/0/223	4062/0/196	4045/0/223	4594/0/262	4637/0/250
GOF on F^2	0.814	1.018	1.011	0.783	1.108	1.012	0.946	1.021
final R indices [$I > 2\sigma$ (I)]	R1 = 0.0385	R1 = 0.0226	R1 = 0.0219	R1 = 0.0642	R1 = 0.0560	R1 = 0.0562	R1 = 0.0263	R1 = 0.0303
	wR2 = 0.0697	wR2 = 0.0516	wR2 = 0.0456	wR2 = 0.1412	wR2 = 0.1578	wR2 = 0.1494	wR2 = 0.0585	wR2 = 0.0763
R indices (all data)	R1 = 0.0385	R1 = 0.0302	R1 = 0.0289	R1 = 0.1309	R1 = 0.0719	R1 = 0.0764	R1 = 0.039	R1 = 0.0374
	wR2 = 0.0697	wR2 = 0.0532	wR2 = 0.0485	wR2 = 0.1538	wR2 = 0.1656	wR2 = 0.1673	wR2 = 0.0595	wR2 = 0.0778
largest diff. peak and hole (e•Å^{-3})	0.608/−0.479	1.164/−0.774	1.069/−0.658	0.801/−0.918	2.065/ −0.892	1.923/−1.978	1.633/−0.481	1.505/−0.618

plexes, guanidinate ligands bearing sterically very bulky substituents like cyclohexyl [Cy], trimethylsilyl [$SiMe_3$], bis(trimethylsilyl)amido [$N(SiMe_3)_2$], and diphenylamido [NPh_2] were used, since the compounds were designed as homogeneous catalysts for different polymerization processes. Because of the high molecular masses of these compounds and the extreme steric crowding of the metal center, low volatility and reactivity are expected.

In this paper, we report the synthesis of a series of eight new homoleptic tris-guanidinate rare-earth complexes $M[(N^iPr)_2CNR_2]_3$ (M = Y, Gd, Dy; R = Me, Et, ^{i}Pr), where the steric demand and molecular mass of the guanidinato ligands were kept as low as possible. All compounds were characterized by X-ray single crystal analysis, elemental analysis (EA), nuclear magnetic resonance (NMR), mass spectrometry (MS) and infrared spectroscopy (IR). The influence of the steric bulk of the dialkylamido group attached to the guanidinate backbone on the volatility of the corresponding complex was studied using thermal analysis (TGA/DTA and isothermal studies). Furthermore, results of the preliminary MOCVD and ALD experiments for the deposition of Dy_2O_3 and Gd_2O_3 are presented.

Experimental Section

General Considerations. All reactions and manipulations of air and moisture-sensitive compounds were performed employing a conventional vacuum/argon line using standard Schlenk techniques. Sample preparation for further analysis was carried out in an argon filled glovebox. All solvents (technical grade) were dried and purified by an MBraun solvent purification system and stored over molecular sieves (4 Å). The NMR-solvents were degassed and dried over activated molecular sieves. The starting compounds: YCl_3 (Alfa Aesar), $GdCl_3$ (ABCR), $DyCl_3$ (ChemPur), *N*,*N*′-diisopropylcarbodiimide (Acros), ^{n}BuLi (Fluka), Et_2NH (Fluka), $^iPr_2NH$ (Aldrich) and Me_2NLi (Aldrich) were used as received. The lithium dialkylamides: Et_2NLi and $^iPr_2NLi$ as well as the lithium *N*,*N*′-diisopropyl-2-dialkylamido-guanidinato ligands $[Li(^iPrN)_2CNR_2]$ were synthesized following modified literature procedures.[46,47]

Physical Measurements. ^{1}H and ^{13}C NMR-spectra were recorded on a Bruker Advance DRX 250 spectrometer. Elemental analysis was performed by the analytical service of the Chemistry Department at the Ruhr-University Bochum (CHNSO Vario EL 1998). Electronic ionization (EI) mass spectra were recorded, using a Varian MAT spectrometer. The IR spectra were recorded using a Bruker ALPHA FT-IR spectrometer. The thermal analysis data were obtained on a Seiko TGA/DTA 6300S11 instrument. The measurements were carried out in aluminum crucibles (closed with an Al lid that has a hole with an area 1.5 mm^2) with approximately 10 mg of sample; the employed heating rate was 5 °C/min and a nitrogen flow (N_2 99.9999%) of 300 mL/min was used.

(42) Zhou, L.; Yao, Y.; Zhang, Y.; Xue, M.; Chen, J.; Shen, Q. *Eur. J. Inorg. Chem.* **2004**, 2167.
(43) Chen, J.-L.; Yao, Y.-M.; Luo, Y.-J.; Zhou, L.-Y.; Zhang, Y.; Shen, Q. *J. Organomet. Chem.* **2004**, *689*, 1019.
(44) Pang, X.; Sun, H.; Zhang, Y.; Shen, Q.; Zhang, H. *Eur. J. Inorg. Chem.* **2005**, 1487.
(45) Zhou, L; Yao, Y.; Zhang, Y.; Sheng, H.; Xue, M.; Shen, Q. *Appl. Organomet. Chem.* **2005**, *19*, 398.
(46) Bradley, D. C.; Thomas, I. M. *J. Chem. Soc.* **1960**, 3857.
(47) Aeilts, S. L.; Coles, M. P.; Swenson, D. C.; Jordan, R. F.; Young, V. G. J. *Organometallics* **1998**, *17*, 3265.

Yttrium Tris(*N*,*N*′-diisopropyl-2-dimethylamido-guanidinate) [Y(^{i}Pr-Me$_2$N-guan)$_3$] (1a). A slurry of $LiNMe_2$ (1.172 g, 18 mmol) in 30 mL of Et_2O was cooled to 0 °C and *N*,*N*′-diisopropylcarbodiimide (2.81 mL, 18 mmol) dissolved in Et_2O (20 mL) was added dropwise. This mixture was allowed to warm to room temperature and stirred for 18 h under inert atmosphere. The resulting pale yellow solution of $[Li(N^iPr)_2CNMe_2]$ was cooled to 0 °C and slowly added to a suspension of YCl_3 (0.992 g, 6 mmol) in Et_2O (60 mL). After warming to room temperature, the reaction mixture was stirred overnight under argon. The solvent was removed under reduced pressure and the product was extracted in hexane, which was then filtered through a celite pad to afford a pale yellow solution. A saturated solution was formed by removing part of the hexane under vacuum and this solution was cooled to −20 °C to afford colorless crystals suitable for single crystal X-ray analysis. Spectroscopically pure white crystalline compound was obtained through sublimation at 120 °C (6×10^{-2} mbar). Yield 2.63 g (73% based on YCl_3). Anal. Calcd. (%) for $C_{27}H_{60}N_9Y$: C, 54.07; H, 10.08; N, 21.02. Found (%): C, 54.01; H, 9.78; N, 21.43. ^{1}H NMR (250 MHz, C_6D_6, RT) δ 3.60 [doublet of septet, J = 1.7 Hz, 6.4 Hz, 6H, $(NCH(CH_3)_2)_2CNMe_2$], 2.63 [s, 18H, $(N^iPr)_2CN(CH_3)_2$], 1.49 [d, J = 6.3 Hz, 18H, $(NCH(CH_3)_2)_2CNMe_2$], 1.30 [d, J = 6.2 Hz, 18H, $(NCH(CH_3)_2)_2CNMe_2$]. ^{13}C NMR (63 MHz, C_6D_6, RT) δ 174.92 $[(N^iPr)_2CNMe_2]$, 49.19 $[(NCH(CH_3)_2)_2CNMe_2]$, 42.93 $[(N^iPr)_2CN(CH_3)_2]$, 29.70 $[(NCH(CH_3)_2)_2CNMe_2]$, 29.21 $[(NCH(CH_3)_2)_2CNMe_2]$. EI-MS (70 eV) [fragment, rel. intensity (%), $M^+ = YL_3^+$] m/z = 598 [YL_3^+, 34%], 555 [YL_3^+-^{i}Pr, 2%], 512 [YL_3^+ - 2 × ^{i}Pr, 0.5%], 428 [YL_2^+, 100%], 384 [YL_2^+ - NMe_2, 40%], 342 [YL_2^+ - NMe_2 - ^{i}Pr, 7%], 301 [YL_2^+ - NMe_2 - 2 × ^{i}Pr, 8%], 258 [YL^+, 13%], 216 [YL^+ - ^{i}Pr, 2%], 171 [$L^+ = {}^i$PrNC(NMe$_2$)N^{i}Pr$^+$, 4%], 114 [^{i}PrN=C(H)-NMe$_2^+$, 10%], 69 [^{i}Pr−N≡C$^+$, 21%], 43 [^{i}Pr, 30%]. IR (KBr, cm^{-1}): 3442(s), 2965(s), 2932(s), 2868(m), 1638(s), 1482(w), 1461(m), 1366(s), 1311(w), 1248(m), 1167(s), 1148(m), 1126(m), 1029(m), 940(s), 725(w), 664(w), 574(m).

All the compounds (**1b**, **c**, **2a**−**c**, **3a**−**c**) were obtained using the same synthetic procedure as for [Y(^{i}Pr-Me$_2$N-GUAN)$_3$] **1a** unless described otherwise.

Gadolinium Tris(*N*,*N*′-diisopropyl-2-dimethylamido-guanidinate) [Gd(^{i}Pr-Me$_2$N-guan)$_3$] (1b). Following the same procedure described for **1a**, $GdCl_3$ (1.582 g, 6 mmol) was reacted with $[Li(N^iPr)_2CNMe_2]$ (18 mmol) in Et_2O at 0 °C. After 48 h of stirring at room temperature under inert atmosphere and the work up described above, the product was obtained as a white crystalline solid. Crystals suitable for single crystal X-ray analysis were obtained from concentrated Et_2O solution. Sublimation temperature: 130 °C (6×10^{-2} mbar). Yield 3.05 g (76% based on $GdCl_3$). Anal. Calcd. (%) for $C_{27}H_{60}N_9Gd$: C, 48.54; H, 9.05; N, 18.87. Found (%): C, 48.25; H, 8.56; N, 19.15. EI-MS (70 eV) [fragment, rel. intensity (%), $M^+ = GdL_3^+$] m/z = 668 [GdL_3^+, 11%], 625 [GdL_3^+-^{i}Pr, 3%], 497 [GdL_2^+, 44%], 453 [GdL_2^+ - NMe_2, 29%], 410 [GdL_2^+ - NMe_2 - ^{i}Pr, 12%], 367 [GdL_2^+ - NMe_2 - 2 × ^{i}Pr, 55%], 327 [GdL^+, 100%], 284 [GdL^+ - ^{i}Pr, 9%], 114 [^{i}PrN=C(H)-NMe$_2^+$, 2%], 69 [^{i}Pr−N≡C$^+$, 4%], 43 [^{i}Pr, 7%], [L = ^{i}PrNC(NMe$_2$)N^{i}Pr]. IR (KBr, cm^{-1}): 3442(s), 2966(s), 2870(s), 1638(s), 1459(m), 1383(s), 1366(s), 1311(w), 1283(w), 1167(s), 1147(m), 1126(m), 1058(w), 1029(m), 940(s), 670(w), 569 (m).

Dysprosium Tris(*N*,*N*′-diisopropyl-2-dimethylamido-guanidinate) [Dy(^{i}Pr-Me$_2$N-guan)$_3$] (1c). The reaction of $DyCl_3$ (1.613 g, 6 mmol) with $[Li(N^iPr)_2CNMe_2]$ (18 mmol) afforded white crystalline product after the work up described for **1a**. Sublimation temperature: 135 °C (6×10^{-2} mbar). Yield 3.26 g (81% based on $DyCl_3$). Anal. Calcd. (%) for $C_{27}H_{60}N_9Dy$: C, 48.16; H, 8.98; N, 18.72. Found (%): C, 47.5; H, 8.4; N, 18.72. ^{1}H NMR (250 MHz,

C_6D_6, RT) δ 15.93 [s, 18H, $(N^iPr)_2CN(CH_3)_2$], −1.29 [br m, 18H, $(NCH(CH_3)_2)_2CNMe_2$], −27.1 [br m, 6H, $(NCH(CH_3)_2)_2CNMe_2$], −29.19 [br m, 18H, $(NCH(CH_3)_2)_2CNMe_2$]. EI-MS (70 eV) [fragment, rel. intensity (%), $M^+ = DyL_3^+$] *m/z* = 674 [DyL_3^+, 18%], 631 [DyL_3^+- ^{i}Pr, 1%], 504 [DyL_2^+, 33%], 460 [DyL_2^+ - NMe_2, 15%], 417 [DyL_2^+ - NMe_2 - ^{i}Pr, 3%], 375 [DyL_2^+ - NMe_2 - 2 × ^{i}Pr, 7%], 333 [DyL^+, 8%], 290 [DyL^+ - ^{i}Pr, 2%], 171 [$L^+ = {}^i$PrNC$(NMe_2)N^i$Pr$^+$, 13%], 114 [^{i}PrN=C(H)-NMe_2^+, 40%], 69 [^{i}Pr−N≡C^+, 100%], 43 [^{i}Pr,29%]. IR (KBr, cm^{-1}): 3443(s), 2965(s), 2869(m), 1638(s), 1462(m), 1383(s), 1367(s), 1311(w), 1249(m), 1167(m), 1147(m), 1126(m), 1058(w), 1029(m), 940(w), 798(w), 724(w), 672(w), 572(m).

Yttrium Tris(*N,N′*-diisopropyl-2-diethylamido-guanidinate) [Y(^{i}Pr-Et$_2$N-guan)$_3$] (2a). YCl_3 (1.172 g, 6 mmol) and $[Li(^iPrN)_2CNEt_2]$ (18 mmol) were reacted according to the synthetic route presented for **1a**. The product was a white crystalline solid. Sublimation temperature: 155−160 °C (6 × 10^{-2} mbar). Yield 2.59 g (63% based on YCl_3). Anal. Calcd. (%) for $C_{33}H_{72}N_9Y$: C, 57.96; H, 10.61; N, 18.43. Found (%): C, 57.03; H, 11.29; N, 17.59. ^{1}H NMR (250 MHz, C_6D_6, RT) δ 3.58 [doublet of septet, J = 1.7 Hz, 6.4 Hz, 6H, $(NCH(CH_3)_2)_2CNEt_2$], 3.17−2.82 [m, 12H, $(N^iPr)_2CN(CH_2CH_3)_2$, AB-part of ABX_3, J_{AB} = −14.05 Hz, J_{AX} = 7.25 Hz, J_{BX} = 7.10 Hz, δ_A = 3.050, δ_B = 2.921], 1.47 [d, J = 6.4 Hz, 18H, $(NCH(CH_3)_2)_2CNEt_2$], 1.33 [d, J = 6.3 Hz, 18H, $(NCH(CH_3)_2)_2CNEt_2$], 0.98 [t, 18H, $(N^iPr)_2CN(CH_2CH_3)_2$, X-Part of ABX_3 (see above)]. ^{13}C NMR (63 MHz, C_6D_6, RT) δ 174.87 [$(N^iPr)_2CNEt_2$], 49.54 [$(NCH(CH_3)_2)_2CNEt_2$], 45.77 [$(N^iPr)_2CN(CH_2CH_3)_2$], 29.51 [$(NCH(CH_3)_2)_2CNEt_2$], 29.06 [$(NCH(CH_3)_2)_2CNEt_2$], 16.88 [$(N^iPr)_2CN(CH_2CH_3)_2$]. EI-MS (70 eV) [fragment, rel. intensity (%), $M^+ = YL_3^+$] *m/z* = 682 [YL_3^+, 59%], 653 [YL_3^+- Et, 2%], 640 [YL_3^+ - ^{i}Pr, 3%], 568 [YL_3^+ - ^{i}Pr - NEt_2, 2%], 484 [YL_2^+, 100%], 455 [YL_2^+ - Et, 7%], 441 [YL_2^+ - ^{i}Pr, 45%], 412 [YL_2^+ - NEt_2, 21%], 400 [YL_2^+ - 2 × ^{i}Pr, 5%], 342 [YL_2^+ - 2 × Et - 2 × ^{i}Pr, 16%], 342 [YL_2^+ - NEt_2 - ^{i}PrN or YL_2^+ - Cdi, 7%], 286 [YL^+, 22%], 198 [$L^+ = {}^i$PrNC$(NEt_2)N^i$Pr$^+$, 3%], 141 [^{i}PrN=C=NEt_2^+, 3%], 84 [^{i}PrN=C=NH^+, 35%], 69 [^{i}Pr−N≡C^+, 22%], 56 [$Me_2C{=}N^+$, 76], 43 [^{i}Pr, 42%]. IR (KBr, cm^{-1}): 3452(s), 2966(s), 2931(s), 2869(m), 1637(s), 1466(m), 1399(m), 1379(m), 1365(m), 1342(m), 1307(m), 1282(m), 1166(s), 1146(m), 1125(m), 1091(w), 1067(w), 1048(w), 949(w), 909(w), 799(w), 720(w), 671(w), 571(m).

Gadolinium Tris(*N,N′*-diisopropyl-2-diethylamido-guanidinate) [Gd(^{i}Pr-Et$_2$N-guan)$_3$] (2b). Following the same procedure as described for **1a**, $GdCl_3$ (1.582 g, 6 mmol) was reacted with $[Li(^iPrN)_2CNEt_2]$ (18 mmol) in Et_2O (60 mL) for 48 h. The product was a white crystalline solid. Sublimation temperature: 160 °C (6 × 10^{-2} mbar). Yield 3.56 g (79% based on $GdCl_3$). Anal. Calcd. (%) for $C_{33}H_{72}N_9Gd$: C, 52.69; H, 9.65; N, 16.76. Found (%): C, 53.2; H, 9.78; N, 15.69. EI-MS (70 eV) [fragment, rel. intensity (%), $M^+ = GdL_3^+$] *m/z* = 754 [GdL_3^+, 1%], 725 [GdL_3^+- Et, 0.5%], 711 [GdL_3^+ - ^{i}Pr, 0.7%], 639 [GdL_3^+ - ^{i}Pr - NEt_2, 29%], 553 [GdL_2^+, 8%], 524 [GdL_2^+ - Et, 0.5%], 511 [GdL_2^+ - ^{i}Pr, 7.5%], 481 [GdL_2^+ - NEt_2, 6%], 426 [GdL_2^+ - NEt_2 - ^{i}PrN or GdL_2^+ - Cdi, 100%], 356 [GdL^+, 58%], 141 [^{i}PrN=C=NEt_2^+, 2%], 84 [^{i}PrN=C=NH^+, 3%], 56 [$Me_2C{=}N^+$, 12], 43 [^{i}Pr, 9%], [$L^+ = {}^i$PrNC$(NEt_2)N^i$Pr$^+$]. IR (KBr, cm^{-1}): 3442(s), 2966(s), 2931(s), 2869(m), 1637(s), 1466(m), 1399(m), 1380(m), 1366(m), 1343(m), 1307(w), 1283(m), 1204(w), 1167(m), 1147(m), 1125(m), 1067(w), 1049(w), 989(w), 799(w), 719(w), 699(w), 571(m).

Dysprosium Tris(*N,N′*-diisopropyl-2-diethylamido-guanidinate) [Dy(^{i}Pr-Et$_2$N-guan)$_3$] (2c). The reaction of $DyCl_3$ (1.613 g, 6 mmol) and $[Li(^iPrN)_2CNEt_2]$ (18 mmol) resulted in the formation of a white crystalline solid after work up described above. Sublimation temperature: 160 °C (6 × 10^{-2} mbar). Yield 3.35 g (74% based on $DyCl_3$). Anal. Calcd. (%) for $C_{33}H_{72}N_9Dy$: C, 52.33; H, 9.58; N, 16.64. Found (%): C, 52.69; H, 10.35; N, 16.48. ^{1}H NMR (250 MHz, C_6D_6, RT) δ 18.35 [br m, 6H, $(N^iPr)_2CN(CH_2CH_3)_2$], 11.89 [br m, 6H, $(N^iPr)_2CN(CH_2CH_3)_2$], 5.11 [br m, 18H, $(N^iPr)_2CN(CH_2CH_3)_2$], −8.13 [br m, 18H, $(NCH(CH_3)_2)_2CNEt_2$], −14.15 [br m, 18H, $(NCH(CH_3)_2)_2CNEt_2$], −36.04 [br m, 6H, $(NCH(CH_3)_2)_2CNEt_2$]. EI-MS (70 eV) [fragment, rel. intensity (%), $M^+ = DyL_3^+$] *m/z* = 758 [DyL_3^+, 3%], 729 [DyL_3^+- Et, 1.2%], 715 [DyL_3^+ - ^{i}Pr, 2.5%], 644 [DyL_3^+ - ^{i}Pr - NEt_2, 2.4%], 615 [DyL_3^+ - ^{i}PrN=C(H)-NEt_2, 1.5%], 559 [DyL_2^+, 18%], 530 [DyL_2^+ - Et, 2%], 516 [DyL_2^+ - ^{i}Pr, 15%], 488 [DyL_2^+ - NEt_2, 12%], 473 [DyL_2^+ - 2 × ^{i}Pr, 2%], 444 [DyL_2^+ - 2 × Et - 2 × ^{i}Pr, 4%], 432 [DyL_2^+ - NEt_2 - ^{i}PrN or DyL_2^+ - Cdi, 100%], 359 [DyL^+, 37%], 141 [^{i}PrN=C=NEt_2^+, 0.4%], 84 [^{i}PrN=C=NH^+, 1%], 69 [^{i}Pr−N≡C^+, 0.5%], 43 [^{i}Pr, 2%], [$L^+ = {}^i$PrNC$(NEt_2)N^i$Pr$^+$]. IR (KBr, cm^{-1}): 3406(s), 2965(s), 2930(s), 2868(s), 1637(s), 1468(s), 1400(m), 1377(s), 1365(m), 1342(m), 1307(m), 1282(m), 1214(w), 1166(m), 1146(m), 1124(m), 1090(m), 1058(w), 990(w), 964(w), 925(w), 861(w), 838(w), 798(w), 686(w), 568(m).

Yttrium Tris(*N,N′*-diisopropyl-2-diisopropylamido-guanidinate) [Y(^{i}Pr-^{i}Pr$_2$N-guan)$_3$] (3a). YCl_3 (1.172 g, 6 mmol) and $[Li(^iPrN)_2CN^iPr_2]$ (18 mmol) were reacted according to the synthetic route presented for **1a**. The product was a white crystalline solid. Yield 3.13 g (68% based on YCl_3). Anal. Calcd. (%) for $C_{39}H_{84}N_9Y$: C, 60.99; H, 11.02; N, 16.41. Found (%): C, 60.35; H, 10.54; N, 16.28. ^{1}H NMR (250 MHz, C_6D_6, RT) δ 3.77 [doublet of septet, J = 1.9 Hz, 6.4 Hz, 6H, $(NCH(CH_3)_2)_2CN^iPr_2$], 3.55 [sept, J = 6.9 Hz, 6H, $(N^iPr)_2CN(CH(CH_3)_2)_2$], 1.47 [d, J = 6.4 Hz, 18H, $(NCH(CH_3)_2)_2CN^iPr_2$], 1.36 [d, J = 6.3 Hz, 18H, $(NCH(CH_3)_2)_2CN^iPr_2$], 1.31 [d, J = 7.0 Hz, 18H, $(N^iPr)_2CN(CH(CH_3)_2)_2$], 1.22 [d, J = 6.7 Hz, 18H, $(N^iPr)_2CN(CH(CH_3)_2)_2$]. ^{13}C NMR (63 MHz, C_6D_6, RT) δ 173.35 [$(N^iPr)_2CN^iPr_2$], 49.54 [$(NCH(CH_3)_2)_2CN^iPr_2$], 46.12 [$(N^iPr)_2CN(CH(CH_3)_2)_2$], 26.65 [$(NCH(CH_3)_2)_2CN^iPr_2$], 26.20 [$(NCH(CH_3)_2)_2CN^iPr_2$], 25.10 [$(N^iPr)_2CN(CH(CH_3)_2)_2$], 22.25 [$(N^iPr)_2CN(CH(CH_3)_2)_2$]. EI-MS (70 eV) [fragment, rel. intensity (%), $M^+ = YL_3^+$] *m/z* = 767 [YL_3^+, 0.8%], 725 [YL_3^+ - ^{i}Pr, 4.4%], 668 [YL_3^+ - N^iPr_2, 0.9%], 625 [YL_3^+ - N^iPr_2 - ^{i}Pr, 1.2%], 541 [YL_2^+, 1.6%], 497 [YL_2^+ - ^{i}Pr, 9.4%], 441 [YL_2^+ - N^iPr_2, 4.6%], 413 [YL_2^+ - ^{i}PrNCN^iPr, 3.4%], 397 [YL_2^+ - N^iPr_2 - ^{i}Pr, 2.2%], 314 [YL^+, 5.8%], 228 [$LH^+ = {}^i$PrNC$(N^iPr_2)N^i$Pr.H, 0.1%], 184 [L^+ - ^{i}Pr, 66%], 127 [(^{i}PrNCN^iPr -H)$^+$, 11%], 100 [^{i}Pr$_2N^+$, 30%], 84 [^{i}PrNCNH$^+$, 50%], 69 [^{i}PrN'C$^+$, 100%], 56 [$(CH_3)_2C{=}N^+$, 43%], 44 [$CH_3CH_2CH_3^+$, 69%]. IR (KBr, cm^{-1}): 3454(s), 2966(s), 2931(s), 2869(m), 1632(s), 1466(m), 1416(m), 1376(m), 1363(m), 1327(m), 1236(w), 1209(w), 1162(m), 1139(m), 1123(m), 1051(w), 1035(w), 931(w), 860(w), 835(w), 752(w), 693(w), 572(m).

Gadolinium Tris(*N,N′*-diisopropyl-2-diisopropylamido-guanidinate) [Gd(^{i}Pr-^{i}Pr$_2$N-guan)$_3$] (3b). Following the same procedure as described for **1a**, $GdCl_3$ (1.582 g, 6 mmol) was reacted with $[Li(^iPrN)_2CN^iPr_2]$ (18 mmol) in Et_2O. After 48 h of stirring at room temperature and the work up described above, the product was obtained as a white crystalline solid. Yield 3.80 g (77% based on $GdCl_3$). Anal. Calcd. (%) for $C_{39}H_{84}N_9Gd$: C, 56.01; H, 10.12; N, 15.07. Found (%): C, 57.5; H, 9.74; N, 14.23. EI-MS (70 eV) [fragment, rel. intensity (%), $M^+ = GdL_3^+$] *m/z* = 735 [GdL_3^+ - N^iPr_2, 0.1%], 694 [GdL_3^+ - N^iPr_2 - ^{i}Pr, 0.2%], 610 [GdL_2^+, 1.9%], 566 [GdL_2^+ - ^{i}Pr, 1.4%], 510 [GdL_2^+ - N^iPr_2, 1.0%], 482 [GdL_2^+ - ^{i}PrNCN^iPr, 1.4%], 467 [GdL_2^+ - N^iPr_2 - ^{i}Pr, 0.6%] 383 [GdL^+, 1.8%], 228 [$LH^+ = {}^i$PrNC$(N^iPr_2)N^i$Pr.H, 0.9%], 184 [L^+ - ^{i}Pr, 90%], 127 [(^{i}PrNCN^iPr -H)$^+$, 15%], 100 [^{i}Pr$_2N^+$, 40%], 84 [^{i}PrNCNH$^+$, 70%], 69 [^{i}PrN≡C^+, 100%], 56 [$(CH_3)_2C{=}N^+$, 62%],

44 [$CH_3CH_2CH_3^+$, 76%]. FAB (NBA matrix) [fragment, rel. intensity (%)] m/z = 228 [LH^+ = ^{i}PrNC(N^{i}Pr$_2$)N^{i}Pr.H, 100%], 184 [L+ - ^{i}Pr, 6%], 128 [^{i}PrNCN^{i}Pr$^+$, 1.5%], 101 [^{i}Pr$_2$NH$^+$, 4%]. IR (KBr, cm^{-1}): 3452(s), 2966(s), 2931(m), 2870(s), 1631(s), 1465(m), 1417(m), 1377(m), 1363(m), 1325(m), 1244(m), 1208(m), 1162(m), 1138(m), 1124(w), 1051(w), 1020(w), 985(w), 932(w), 861(w), 668(w), 573 (m).

Dysprosium Tris(*N*,*N*′-diisopropyl-2-diisopropylamido-guanidinate) [Dy(^{i}Pr-^{i}Pr$_2$N-guan)$_3$] (3c). The reaction of $DyCl_3$ (1.613 g, 6 mmol) and [Li(^{i}PrN)$_2$CN^{i}Pr$_2$] (18 mmol) resulted in the formation of a white crystalline solid after work up described above. Yield 3.52 g (70% based on $DyCl_3$). Anal. Calcd. (%) for $C_{39}H_{84}N_9Dy$: C, 55,66; H, 10.06; N, 14.98. Found (%): C, 54.98; H, 9.68; N, 15.07. ^{1}H NMR (250 MHz, C_6D_6, RT) δ 32.10 [br m, 6H, (N^{i}Pr)$_2$CN(C*H*(CH$_3$)$_2$)$_2$], 13.97 [br m, 18H, (N^{i}Pr)$_2$CN(CH(C*H*$_3$)$_2$)$_2$], 11.39 [br m, 18H, (N^{i}Pr)$_2$CN(CH(C*H*$_3$)$_2$)$_2$], −1.73 [br m, 18H, (NCH(C*H*$_3$)$_2$)$_2$CN^{i}Pr$_2$], −27.65 [br m, 6H, (NC*H*(CH$_3$)$_2$)$_2$CN^{i}Pr$_2$], −42.36 [br m, 18H, (NCH(C*H*$_3$)$_2$)$_2$CN^{i}Pr$_2$]. EI-MS (70 eV) [fragment, rel. intensity (%)] m/z = 228 [LH^+ = ^{i}PrNC(N^{i}Pr$_2$)N^{i}Pr.H, 2.1%], 184 [L^+ - ^{i}Pr, 100%], 127 [(^{i}PrNCN^{i}Pr -H)$^+$, 5%], 100 [^{i}Pr$_2$N$^+$, 37%], 84 [^{i}PrNCNH$^+$, 53%], 69 [^{i}PrN≡C$^+$, 32%], 56 [(CH$_3$)$_2$C═N$^+$, 41%], 44 [$CH_3CH_2CH_3^+$, 75%]. CI-MS (NH_3) [fragment, rel. intensity (%), M^+ = DyL_3^+] m/z = 843 [(DyL_3 + H)$^+$, 0.3%], 617 [(DyL_2 + H)$^+$, 0.2%], 228 [LH^+ = ^{i}PrNC(N^{i}Pr$_2$)N^{i}Pr.H, 100%], 184 [L^+ - ^{i}Pr, 61%], 169 [LH^+ - ^{i}PrN≡C, 38%], 127 [(^{i}PrNCN^{i}Pr - H)$^+$, 34%], 102 [^{i}Pr$_2$NH$_2^+$, 41%], 100 [^{i}Pr$_2$N$^+$, 24%]. IR (KBr, cm^{-1}): 3454(s), 2966(s), 2931(s), 2870(m), 1631(s), 1466(m), 1416(m), 1376(m), 1326(m), 1236(w), 1209(w), 1162(m), 1138(m), 1123(m), 1051(w), 1019(w), 931(w), 861(w), 835(w), 777(w), 752(w), 692(w), 572(m).

X-ray Structure Determination. Single crystals of compounds **1a**−**c**, **2a**−**c** and **3b**, **c** were mounted on thin glass capillaries and then cooled to data collection temperature (113 K). Diffraction data were collected on a X-calibur 2 Oxford diffractometer using graphite monochromated Mo Kα radiation (λ = 0.71073 Å). The structure was solved using SHELXL-97 software package and refined by full matrix least-squares methods based on F^2 with all observed reflections.[48] Crystal data and final agreement factors are listed in Table 1. For structures **2a**−**c** and **3b**, **c**, cyclohexane was found in the unit cell. Because of disordered solvent in case of **2b**, we decided to correct the X-ray data employing the SQUEEZE routine in PLATON.[49]

Thin Film Deposition. MOCVD and ALD experiments were performed using **1b** and **1c** as precursors which were handled in a glovebox. Films were grown on ultrasonically cleaned 2-in. *p*-type Si(100) substrates (SI-MAT) without removing the native oxide layer. A home-built, horizontal cold wall low pressure reactor[50] was employed for MOCVD experiments. Nitrogen (flow rate: 50 sccm, 99.9999%) and oxygen (flow rate: 50 sccm, 99.999%) were used as carrier and reactive gases, respectively. For each deposition, approximately 200 mg of the precursor was filled into a glass bubbler in a glovebox. Depositions were carried out in the substrate temperature range of 300 and 700 °C, while the precursor vaporizer was maintained at 130 °C. Depositions were carried out for 30 min and reactor pressure was maintained at 1 mbar.

The ALD experiments were carried out using a commercial flow-type hot-wall ALD reactor (ASM Microchemistry, F-120). Prior to film deposition, about 200 mg of the compound was inserted into the ALD reactor and was evaporated from an open crucible kept at 130 °C. Water was used as an oxidizing agent, which was evaporated from a container maintained at 25 °C. The ALD chamber pressure was maintained at 1−3 mbar during the depositions. Nitrogen (99.9999%, Air Liquide) was used as the carrier as well as purging gas. The following pulsing sequences (ALD growth cycle) were used: 0.5−3 s pulse of Gd precursor, followed by 2−5 s of N_2 purge, 0.5−2 s H_2O, and finally 5−10 s of N_2 purge.

Film Characterization. The crystallinity of the films was investigated by X-ray diffraction (XRD) analyses using a Bruker D8 Advance AXS Diffractometer [Cu Kα radiation (1.5418 Å)] with a position sensitive detector (PSD). All films were analyzed in the $\theta-2\theta$ geometry. The surface morphology of the film was analyzed by scanning electron microscope (SEM) using a LEO Gemini SEM 1530 electron microscope. An Oxford ISIS EDX system coupled with the SEM instrument was used for the energy dispersive X-ray (EDX) analysis.

Results and Discussion

Synthesis and Structures. Following the general synthetic route for the synthesis of lithium guanidinates published by Aeilts et al., the lithiated *N*,*N*′-diisipropyl-guanidinato ligands Li[(N^{i}Pr$_2$)CNR$_2$] used in this work were prepared by the reaction of *N*,*N*′-diisopropylcarbodiimide with three different lithium dialkylamides LiNR$_2$ (R = Me, Et, ^{i}Pr) in Et_2O.[47] Since this reaction gives a nearly quantitative yield of lithiated guanidinato ligand, a freshly prepared solution of the corresponding lithium guanidinate [Li(N^{i}Pr$_2$)CNR$_2$] [R = Me (**1**), Et (**2**), ^{i}Pr (**3**)] was used directly in the subsequent salt metathesis reactions. The treatment of diethyl ether (Et_2O) slurry of MCl_3 [M = Y (**a**), Gd (**b**), Dy (**c**)] with 3 equiv of Li[(N^{i}Pr$_2$)CNR$_2$] afforded a series of new homoleptic tris-*N*,*N*′-diisopropyl-2-dialkylamidoguanidinato rare earth complexes M[(N^{i}Pr)$_2$CNR$_2$]$_3$ (Scheme 2). It should be noted that Y[(N^{i}Pr)$_2$N^{i}Pr$_2$]$_3$ (**3a**) has previously been reported in the literature as a byproduct that was formed by the rearrangement of (C$_5$H$_5$)Y[(N^{i}Pr)$_2$N^{i}Pr$_2$]$_2$ to (C$_5$H$_5$)$_2$Y-[(N^{i}Pr)$_2$N^{i}Pr$_2$] and Y[(N^{i}Pr)$_2$N^{i}Pr$_2$]$_3$,[51] but strictly taken in this case, the complex is a result of carbodiimide insertion and not salt metathesis reaction, which is adopted here for precursor synthesis.

Interestingly, in contrast to the synthesis of the yttrium- (**1a**, **2a**, **3a**) and dysprosium guanidinates (**1c**, **2c**, **3c**), where the metathesis reaction was completed within 24 h, in case of gadolinium guanidinates (**1b**, **2b**, **3b**), 48 h were needed for reaction completion. This could be due to lower solubility of $GdCl_3$ in Et_2O when compared to YCl_3 and $DyCl_3$.

After workup, the rare earth guanidinates **1a**−**c**, **2a**−**c** and **3a**−**c** were isolated in reasonable yields (70−80%) as white crystalline solids. The purification of the products was done by recrystallization and/or sublimation. The compounds have good solubility in common organic solvents like Et_2O, tetrahydrofuran (THF), toluene and hexane.

The molecular structures of **1a**−**c**, **2a**−**c** and **3b**,**c** in the solid state were determined by single crystal X-ray analysis. For compounds **2a**−**c** and **3b**, **c**, cyclohexane was found in the unit cell which comes from the solvent used for crystallization. Since the complexes of the different rare earth metals [Y (**a**), Gd (**b**)

(48) Sheldrick, G. M. *SHELXL-97, Program for the Refinement of the Crystal Structure*, University of Göttingen: Göttingen, Germany, 1997.
(49) Spek, A. L. *Acta Crystallogr., Sect. A* **1990**, *46*, C34.
(50) Devi, A.; Rogge, W.; Wohlfart, A.; Hipler, F.; Becker, H.-W.; Fischer, R. A. *Chem. Vap. Deposition* **2000**, *6*, 245.
(51) Zhang, J; Cai, R.; Weng, L.; Zhou, X. *Organometallics* **2004**, *23*, 3303.

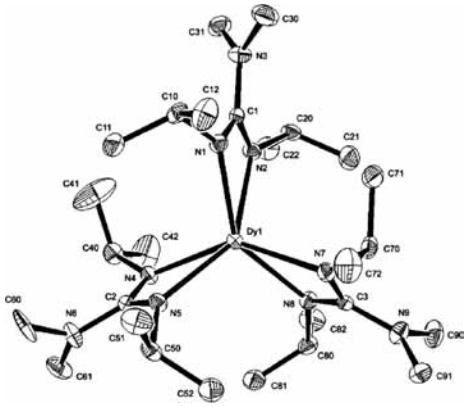

Figure 1. The molecular structure of Dy[(N^{i}Pr)$_2$CNMe$_2$]$_3$ (**1c**) in the solid state. Hydrogen atoms were omitted for clarity and the thermal ellipsoids are shown at 30%.

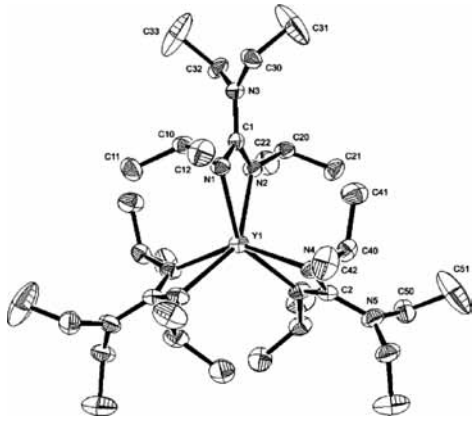

Figure 2. The molecular structure of Y[(N^{i}Pr)$_2$CNEt$_2$]$_3$ (**2a**) in the solid state. Hydrogen atoms were omitted for clarity and the thermal ellipsoids are shown at 30%.

or Dy (**c**)] that have the same dialkyl-guanidinato ligands (**1**, **2** or **3**) are isostructural, only the molecular structures of **1c**, **2a** and **3b** are shown in Figures 1−3 as representative examples. Crystal and structure refinement data for all eight compounds are summarized in Table 1. Selected bond lengths and angles are given in Table 2.

According to the single crystal X-ray analysis, all eight complexes (**1a**−**c**, **2a**−**c**, **3b**,**c**) are monomeric in the solid

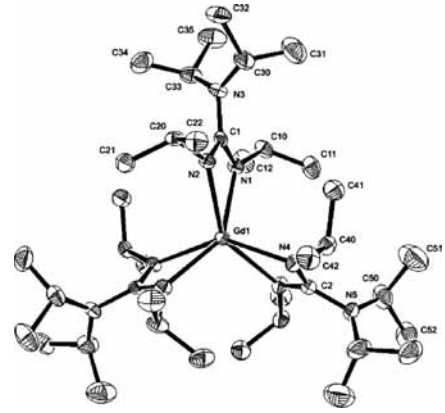

Figure 3. The molecular structure of Gd[(N^{i}Pr)$_2$CN^{i}Pr$_2$]$_3$ (**3b**) in the solid state. Hydrogen atoms were omitted for clarity and the thermal ellipsoids are shown at 30%.

state. The rare earth center in each complex is coordinated to six nitrogen atoms of the three chelating η^2-guanidinato ligands. In order to determine the coordination geometry around the metal, it is reasonable to consider the torsion angle N$_c$−Q1−Q2−N$_x$ between the two planes N$_c$N$_d$N$_f$ and N$_x$N$_y$N$_z$, those that are formed by the six guanidinate backbone N atoms (Q1 and Q2 are the centroids of the two planes, see SI8 in Supporting Information). For ideal trigonal prism and ideal octahedron, these torsion angles are expected to be 0° and 90°, respectively. In case of **1c**, the planes N(1)N(5)N(7) and N(2)N(4)N(8) are nearly parallel with a dihedral angle of 0.4° and the torsion angle N(1)−Q1−Q2−N(2) is 20.17° (Dy-Q1 = 1.056 Å; Dy-Q2 = 1.072 Å). For the other complexes (**1a**−**b**, **2a**−**c**, **3b**−**c**), these planes are also nearly parallel (dihedral angle = 0.1−0.6°) and the torsion angles N$_c$−Q1−Q2−N$_x$ are in the range of 19−21.43° (see Table 2). Thus, the geometry around the rare earth ions can be best described as a distorted trigonal prism. From the data presented in Table 2, it can be seen that, for isostructural complexes bearing identical guanidinate ligands, the torsion angle N$_c$−Q1−Q2−N$_x$ increases in the order Gd[(N^{i}Pr)$_2$CNR$_2$]$_3$ < Dy[(N^{i}Pr)$_2$CNR$_2$]$_3$ < Y[(N^{i}Pr)$_2$CNR$_2$]$_3$. This could be explained with increased steric interacion of the guanidinate ligands in the same order, which results from the

Table 2. Selected Bond Lengths and Angles for **1a**−**c**, **2a**−**c** and **3b**, **c**[a]

	1a	1b	1c	2a	2b	2c	3b	3c
				Mean Bond Lengths (Å)				
M−N^a	2.368(3)	2.410(7)	2.379(5)	2.377(8)	2.406(9)	2.377(5)	2.405(4)	2.384(8)
C−N^a	1.334(8)	1.335(7)	1.333(4)	1.338(6)	1,329(14)	1.323(14)	1.334(5)	1.335(5)
C−N^b	1.396(8)	1.396(8)	1.397(4)	1.412(8)	1.403(17)	1.403(12)	1.408(8)	1.419(10)
				Bond Angles (deg)				
N^a−M−N^a	56.74(8)	55.90(7)	56.56(7)	56.93(15)	55.62(17)	56.30(19)	55.69(7)	56.37(9)
	56.93(8)	55.82(7)	56.55(8)	56.60(2)	55.9(2)	56.10(2)	56.04(10)	56.54(13)
	56.95(8)	55.83(7)	56.60(8)	–	–	–	–	–
N^a−C−N^a	115.2(2)	114.7(2)	116.0(2)	115.8(5)	116.2(5)	116.4(6)	115.2(2)	115.6(3)
	115.7(2)	116.3(2)	115.1(2)	114.9(6)	114.1(7)	114.2(7)	114.7(3)	114.2(4)
	115.3(2)	115.3(2)	115.1(2)	–	–	–	–	–
				Torsion Angles (deg)				
N^a−C−N^b−C	38.08	36.31	41.71	47.66	46.49	46.62	56.96	57.83
	43.85	39.61	38.32	46.72	45.00	45.26	57.69	58.17
	40.95	44.04	43.96	–	–	–	–	–
N$_c$−Q1−Q2-N$_x$	20.77	19	20.17	21.43	19.47	20.55	20.26	21.34

[a] N^a = N(^{i}Pr)-; N^b = -N(Me$_2$); Q1 and Q2 centroids of the planes N$_c$N$_d$N$_f$ and N$_x$N$_y$N$_z$.

Table 3. Overview of the Fragments of Complexes **1a−c** Observed in the Mass Spectra[a]

	1a		1b		1c	
fragment	mass (*m*/*z*)	rel. int. (%)	mass (*m*/*z*)	rel. int. (%)	mass (*m*/*z*)	rel. int. (%)
ML_3^+	598	34	668	11	674	18
ML_3^+ - ^{i}Pr	555	2	625	3	631	1
ML_3^+ - 2× ^{i}Pr	512	0.5	n.d.	–	n.d.	–
ML_2^+	428	100	497	44	504	33
ML_2^+ - NMe_2	384	40	453	29	460	15
ML_2^+ - ^{i}Pr - NMe_2	381	7	410	12	417	3
ML_2^+ -2× ^{i}Pr - NMe_2	301	8	367	55	375	7
ML^+	258	13	327	100	333	8
ML^+ - ^{i}Pr	216	2	284	9	290	2
L^+	171	4	n.d.	–	171	13
^{i}PrN=C(H)-NMe_2	114	10	114	2	114	40
^{i}Pr−N≡C	69	21	69	4	69	100
^{i}Pr$^+$	43	30	43	7	43	29

[a] M = Y, Gd, Dy; L = ^{i}PrNC(NMe_2)N^{i}Pr.

decrease of the ionic radius of the six coordinated rare earth ions [Gd^{3+}(0.938 Å) > Dy^{3+}(0.912 Å) > Y^{3+} (0.900 Å)].[52] Furthermore, an increase in the degree of geometry distortion with increased steric bulk of the dialkylamido group (Me_2N < Et_2N < $^i Pr_2N$) of the guanidinate ligand is also evident. The average M−N bond lengths in **1a−c**, **2a−c**, **3b−c** range from 2.368(3) to 2.410(7) Å (see Table 2). Again, due to the difference in the ionic radii of the rare earth ions, the average Gd−N bonds lengths are significantly larger than the average Y−N and Dy−N bond lengths.

These values are comparable to those for the homoleptic tris-guanidinate complexes Tb[(N^{i}Pr)$_2$CN^{i}Pr$_2$]$_3$ (2.393 Å),[44] Nd[(N^{i}Pr)$_2$CN^{i}Pr$_2$]$_3$ (2.464 Å),[43] Nd[(NCy)$_2$CN^{i}Pr$_2$]$_3$ (2.458 Å),[43] Sm[(NCy)$_2$CNPh_2]$_3$ (2.442 Å),[42] Nd[(NCy)$_2$CNPh_2]$_3$ (2.479 Å)[42] and Yb[(NCy)$_2$CNPh_2]$_3$·2PhCH_3 (2.375 Å),[45] when the difference in the ionic radii of Nd, Sm, Tb and Yb is considered. As expected, the four-membered MNCN chelate rings are essentially planar with N−M−N and N−C−N bond angles similar for all eight complexes **1a−c**, **2a−c**, **3b−c** (see Table 2) and comparable to those reported in the literature.[42−45] The C−N(guan) distances within the chelating guanidinate ligands are significantly shorter than a C−N single bond, which reflects the π-electron delocalization within the NCN unit. The IR spectra of these complexes exhibit strong absorptions in the range of 1630−1640 cm^{-1}, which are consistent with a partial C=N double bond character. This supports the X-ray data, indicating that the π-electrons are delocalized within the NCN-linkage. The question regarding the conjugation of the p-orbital of the N(R_2)-center with the π-system of the NCN-moiety in the guanidinate ligand and the particular contributions of the resonance forms **B** and **C** (Scheme 1) could be discussed considering two parameters. In case of a significant conjugation, the NR_2-function should be sp^2-hybridized, allowing the donation of the lone pair localized on the non hybridized p-orbital into the NCN electronic system. In addition, there should be a minimal torsion angle between the plane of the NR_2-function and that defined by the NCN chelate (optimal π-orbital overlap). As revealed from the single crystal X-ray analysis, the corresponding NR_2-functions of complexes **1a−c**, **2a−c**, **3b−c** are nearly planar with sum of the bonding angles around the respective N-atoms of almost 360°, which points to the particular sp^2-hybridization of these nitrogen centers. The torsion angle N(guan)−C−N(amide)−C between the plane NR_2-function and the NCN moieties for the guanidinate ligand is in the range from 36.31 to 57.83°. According to data presented in Table 2, a gradual increase of this torsion angle with increased steric bulk of the dialkylamido group is observed. This shows that for **1a−c**, **2a−c**, and **3b−c**, the conjugation (π-overlap) between the exocyclic nitrogen and the NCN chelate decreases as the steric bulk of the NR_2 substituent increases and the NR_2 unit twists more out of the RN-C-NR plane. Thus, the corresponding structures of the guanidinate ligands in **1a−c**, **2a−c**, **3b−c** can be rationalized between the limiting forms **B** and **C** shown in Scheme 1, with contribution of the resonance structure **C** that is decreasing in the order M[(N^{i}Pr)$_2$CNMe_2]$_3$ (**1a−c**) > M[(N^{i}Pr)$_2$CNEt_2]$_3$ (**2a−c**) > M[(N^{i}Pr)$_2$CN^{i}Pr$_2$]$_3$ (**3b−c**).

The M[(N^{i}Pr)$_2$CNR_2]$_3$ complexes **1a−c**, **2a−c**, **3a−c** were further characterized using NMR spectroscopy. The ^{1}H NMR spectra of the yttrium tris-guanidinates (**1a**, **2a**, **3a**) show that the monomeric structure of the complexes is also retained in solution. The spectra of **1a** and **2a** display one equivalent environment for the three ^{i}Pr-Me_2N-guanidinato and the ^{i}Pr-Et_2N-guanidinato ligands. In both cases, the ^{i}Pr-groups show a doublet of septet for the CH-protons (3.60 ppm **1a**, 3.58 ppm **2a**), which is due to the coupling of this protons with the yttrium center as well as two well-resolved doublets having equal intensity for the methyl moieties (1.49 ppm and 1.30 ppm **1a**; 1.47 ppm and 1.33 ppm **2a**). The appearance of only one singlet for the dimethylamido group in **1a** (2.63 ppm) is consistent either with the free rotation of the C-NMe_2 bond at room temperature or with a fast racemization of the complex via Bailar like twist. Similarly for **2a**, only one triplet for the CH_3-protons (0.98 ppm) and multiplet for the diastereotopic CH_2-protons (3.17−2.82 ppm) of the C-NEt_2 group are observed. The ^{1}H NMR spectrum of **3a** shows one doublet of septet and a binomial septet in 1:1 ratio corresponding to the CH- protons of the ^{i}Pr- groups of the guanidinate backbone (3.77 ppm, 6H) and the $^i Pr_2$N-group (3.55 ppm, 6H), respectively. Additionally, four doublets of equal integral area at 1.47 ppm (18 H), 1.36 ppm (18H), 1.31 ppm (18H) and 1.22 ppm (18H) that correspond to the diastereotopic CH_3-protons of the (^{i}PrN)$_2$C- and $^i Pr_2$N-groups are observed. In contrast, for the same compound [obtained as a byproduct by the synthesis of Cp_2Y(N^{i}Pr)$_2$CN^{i}Pr$_2$], Zhang et al. reported a quite confusing ^{1}H NMR spectrum, which consists of only one multiplet at 3.57 ppm (12H) and three doublets in 1:1:1 ratio at 1.36 ppm (24H), 1.20 ppm (24H) and 0.91 ppm (24H), respectively.[51] If one assumes that due to higher temperature or a certain exchange mechanism the two different CH-protons of the (^{i}PrN)$_2$C- and $^i Pr_2$N-groups could appear as one multiplet (though unlikely), then, for the CH_3-protons either three doublets of the ratio

(52) Shannon, R. D. *Acta Crystallogr.* **1976**, *A32*, 751.

Table 4. Physical Properties of Rare Earth Guanidinato Complexes **1a**−**c**

complex	sublimation temperature*	TG-residue	evaporation rate (μg min^{-1} cm^{-2})				half-life (days)			
			100 °C	120 °C	140 °C	160 °C	100 °C	140 °C	180 °C	220 °C
Y[(N^{i}Pr)$_2$CNMe$_2$]$_3$ **1a**	120 °C	6%	7.77	10.1	12.0	16.2	137	102	83	5.21
Gd[(N^{i}Pr)$_2$CNMe$_2$]$_3$ **1b**	130 °C	10%	6.17	7.94	11.31	17.12	–	–	–	–
Dy[(N^{i}Pr)$_2$CNMe$_2$]$_3$ **1c**	135 °C	10%	5.7	9.4	13.5	17.4	965	404	159	1.39

* Sublimation pressure 6×10^{-2}mbar (ca. 0.05 Torr).

1:1:2 (18H:18H:36H) or only two doublets of 1:1 ratio can be expected, but not three doublets in 1:1:1 ratio (24H: 24H:24H) as reported by Zhang et al..

The ^{1}H NMR spectra of the dysprosium tris-guanidinates (**1c**, **2c**, **3c**) have large shifts and broad peaks, which is consistent with the fact that they are paramagnetic. The numbers of peaks and their integral areas are consistent with monomeric structures in solution. Similar considerations like in the case of yttrium tris-guandinates can also be employed here. Despite several attempts, we failed to obtain resolved ^{1}H NMR spectrum of the gadolinium containing complexes (**1b**, **2b** and **3b**) and only a very broad signal from 4 ppm to −5 ppm was observed. But since these complexes are isostructural to the Y- and Dy-guanidinates (**1a**,**c**; **2a**,**c**;**3a**,**c**) a similar solution behavior is expected.

Additional characterization of complexes **1a**−**c**, **2a**−**c**, **3a**−**c** was carried out employing electron impact mass spectrometry (EI-MS, 70 eV). Interestingly, for the isostructural complexes, very similar fragmentation patterns were obtained, which show that these complexes decompose in a similar pathway under mass-spectrometric conditions. In the following, the fragmentation of the Me$_2$N-guandinato complexes M[(N^{i}Pr)$_2$CNMe$_2$]$_3$ (**1a**−**c**) will be discussed in detail, since these complexes show a clear fragmentation pattern, which allows us to propose a plausible decomposition mechanism. All fragments observed in the EI-MS spectra of **1a**−**c** are summarized in Table 3.

In all three fragmentation patterns, the molecular ion peaks (M^+) with an intensity of 34% (**1a**), 11% (**1b**) and 18% (**1c**) were detected. Since no peaks with higher *m*/*z* were observed, the suggested monomeric structure of **1a**−**c** could be confirmed. The first fragmentation step observed can be assigned to the cleavage of an isopropyl group ($M^+ - 43$) from one of the guanidinato ligands. After the loss of a second ^{i}Pr-moiety from the same guanidinate ligand (observed only in case of **1a**) and subsequent loss of the whole ligand rest, the ML_2^+ fragments for **1a** ($m/z = 428$), **1b** ($m/z = 497$) and **1c** ($m/z = 504$) could clearly be identified. The ML_2^+ fragment decomposes further through the cleavage of a Me$_2$N-group, followed by the subsequent loss of two ^{i}Pr-fragments, probably from one and the same guandinato ligand. Finally, after the rest of the guanidinato ligand is lost, a ML^+ fragment for all the three complexes is observed ($m/z = 258$ **1a**, 327 **1b**, 333 **1c**). Given the potential of complexes **1a**−**c** in vapor-phase thin film fabrication (MOCVD and ALD), it is significant to note that in the mass spectrometry data of these complexes only peaks for the guanidine and no peaks for *N*,*N*′-diisopropylcarbodiimide were observed. This shows that, in contrast to the main group compounds Ga[(N^{i}Pr)$_2$CNMe$_2$]$_3$ and Al[(N^{i}Pr)$_2$CNMe$_2$]$_3$, where carbodiimide deinsertion has been clearly observed,[53] for complexes **1a**−**c**, no carbodiimide deinsertion reaction is taking place.

In comparison, the EI-MS spectra of the ^{i}Pr$_2$N-guanidinato complexes **3a**−**c** show similar fragmentation patterns as observed for **1a**−**c** (see Supporting Information, SI 3). However, apart from the peak at *m*/*z* 184 (Int. 65−90%), which is assigned to a guanidinato ligand fragment, the presence of a peak at *m*/*z* 127−128 (Int. 10−15%) clearly shows the presence of *N*,*N*′-diisopropylcarbodiimide. Thus, deinsertion reactions during the evaporation of complexes **3a**−**c** cannot be ruled out. The EI-MS spectra of M[(N^{i}Pr)$_2$CNEt$_2$]$_3$ (**2a**−**c**) are much more complex than the spectra of **1a**−**c** and **3a**−**c** (see Supporting Information, SI 2); therefore, no explicit decomposition pathway could be proposed. Nevertheless, for all three complexes, the molecular peaks were observed. These results suggest that the complexes are thermally stable and vaporize intact without decomposition. Furthermore, the absence of peaks with *m*/*z* higher than M^+ indicates that **2a**−**c** are monomers in the gas phase.

Although the presented EI-MS spectra of rare earth guanidinato complexes indicate a defined, clean decomposition of the complexes, without presence of carbodiimide deinsertion products, one should keep in mind that this is only true under mass spectrometric conditions, where ionic species are involved. In order to investigate the thermal behavior of the rare earth guanidinates (**1a**−**c**, **2a**−**c**, **3a**−**c**) under CVD and ALD conditions, additional decomposition studies such as matrix isolation are required.

Thermal Properties. As the primary goal of synthesizing tris-guanidinato rare earth compounds was driven by our interest to use them as precursors for MOCVD and ALD of rare earth oxide films, sublimation experiments, thermogravemetric analysis (TGA) and isothermal studies were employed to investigate the volatility and thermal stability of **1a**−**c**, **2a**−**c**, **3a**−**c**. For the ^{i}Pr-Me$_2$N-guanidinates **1a**−**c**, complete sublimation was achieved within few hours at 120−135 °C/0.05 Torr (see Table 4) without any measurable residue or color change. Compared to **1a**−**c**, the sublimation of the ^{i}Pr-Et$_2$N-guanidinates **2a**−**c** requires higher temperatures ($T_{subl.}$ = 150−165 °C/0.05 Torr) in order to be completed within a reasonable time (few hours). Also here, after the sublimation was completed, only a negligible residue was left behind. Preliminary sublimation experiments on **3a**−**c** revealed that temperatures higher than 150−160 °C are required. Since we were interested in precursors that sublime at temperatures lower than 150 °C, sublimation studies of **3a**−**c** were not performed. Thus, in terms of volatility, the M(^{i}Pr-Me$_2$N-guan)$_3$ **1a**−**c** are comparable with

the tris-amidinates Ln(^{i}Pr-Me-AMD)$_3$[28,54] and Ln(^{i}Pr-^{t}Bu-AMD)$_3$[27] ($T_{subl.}$ = 90−125 °C/0.02−0.05 Torr), which are the most volatile rare earth compounds known,[25] and significantly more volatile than the Ln(^{t}Bu-Me-AMD)$_3$ ($T_{subl.}$ > 200 °C/0.05 Torr).[55]

The thermal behavior of **1a**−**c**, **2a**−**c** and **3a**−**c** was further studied by TGA and the TG curves obtained for the M(^{i}Pr-Me$_2$N-guan)$_3$ **1a**−**c** are presented in Figure 4.

As seen in Figure 4, compounds **1a**−**c** exhibit very similar thermal behavior, which is consistent with single step evaporation. For all three precursors, the onset of volatilization (221 °C) and the temperature where the evaporation is completed (ca. 267 °C) are similar. Comparing these data with those reported for Y(^{i}Pr-Me-AMD)$_3$ (onset = ca. 225 °C, evaporation end = 287 °C), it is seen that there is a remarkable similarity in the thermal behavior of the guanidinato- and amidinato- complexes, although the molecular mass of a ^{i}Pr-Me$_2$N-guanidinato complex is approximately 15% higher than the mass of the corresponding ^{i}Pr-Me-amidinate complex, bearing the same rare earth center. This indicates very clearly that not only the molecular mass of a compound, but also other factors like steric crowding, electronic saturation, intermolecular interactions, and so forth have strong influence on its thermal behavior. The residual masses of 6% (**1a**), 10% (**1b**) and 10% (**1c**) are higher than expected based on the sublimation studies. This is very likely due to the fact that the presented TGA-curves were recorded on a TG-machine, which is operated at ambient conditions outside a glovebox. For air sensitive compounds like the rare earth guanidinates, this could lead to partial decomposition and thus to higher residual masses. In fact, a closer look at the TGA-curves in Figure 4 shows a slight, but continuous weight loss, which starts already at the beginning of the measurement. This can be attributed to a slow decomposition of the precursor through reaction with ambient air.

The TGA-curves of **2a**−**c** show also similar behavior among each other, but in contrast to **1a**−**c**, three separate weight loss steps are clearly evident (see Supporting Information, SI 4). Since the onset for the first step is located at very low temperatures (ca. 53 °C), this step arises most probably from precursor decomposition, caused by the short exposure of the TGA-crucible to air. With increasing temperature, a second weight loss step (8−10%) occurs at ca. 118 °C. It could be attributed either to the loss of one or more small functional groups from the precursor (precursor decomposition) or to the loss of solvent (cyclohexane) from the lattice. In fact, for compounds **2a**−**c**, the presence of cyclohexane was confirmed by X-ray analysis, and even after sublimation, the presence of some trace solvent in the sublimed precursors was confirmed by NMR. However, since precursor decomposition at this temperature cannot be ruled out, additional experiments like coupled TGA-MS may give better insight into the decomposition mechanism. Finally,

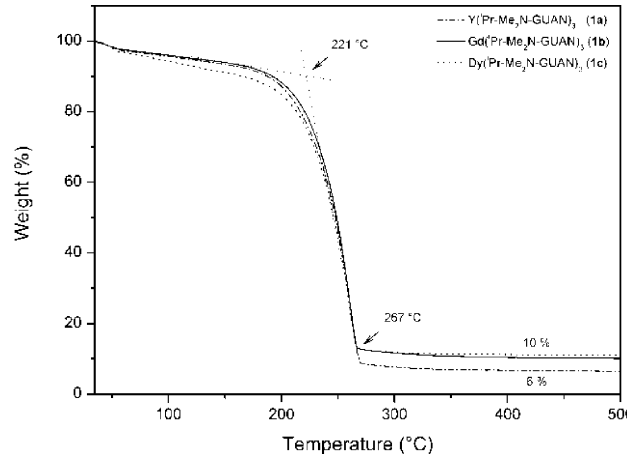

Figure 4. TGA plots of M(^{i}Pr-Me$_2$N-guan)$_3$ (**1a**−**c**).

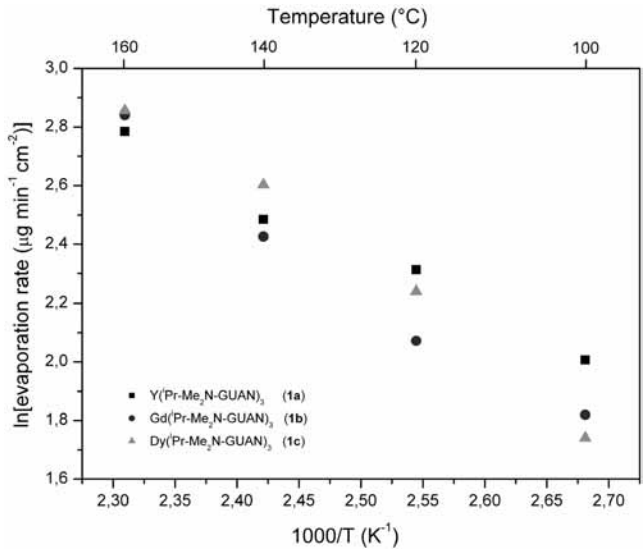

Figure 5. Evaporation rates of the rare earth guanidinates **1a**−**c**.

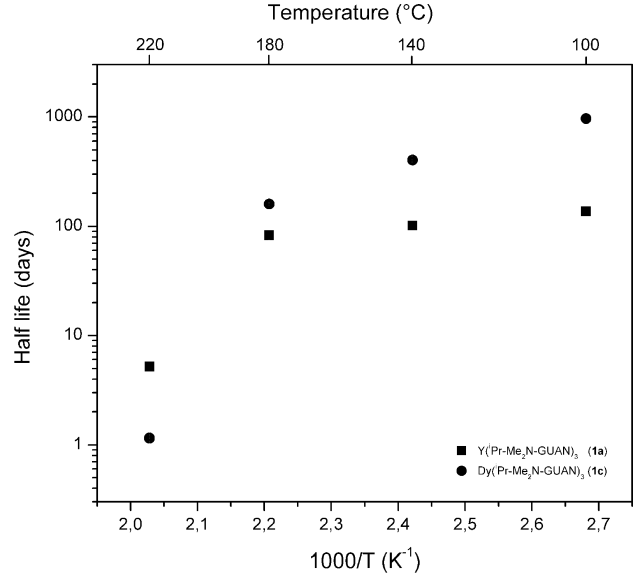

Figure 6. Half-life of the rare earth guanidinates (**1a** and **1c**) at different temperatures in solution.

(53) (a) Kenney, A. P.; Yap, G. P. A.; Richeson, D. S.; Barry, S. T. *Inorg. Chem.* **2005**, *44*, 2926. (b) Brazeau, A. L.; Wang, Z.; Rowley, C. N.; Barry, S. T. *Inorg. Chem.* **2006**, *45*, 2276.
(54) De Rouffignac, P.; Park, J.-S.; Gordon, R. G. *Chem. Mater.* **2005**, *17*, 4808.
(55) Päiväsaari, J.; Dezelah IV, C. L.; Back, D.; El-Kaderi, H. M.; Heeg, M. J.; Putkonen, M.; Niinistö, L; Winter, C. H. *J. Mater. Chem.* **2005**, *15*, 4224.

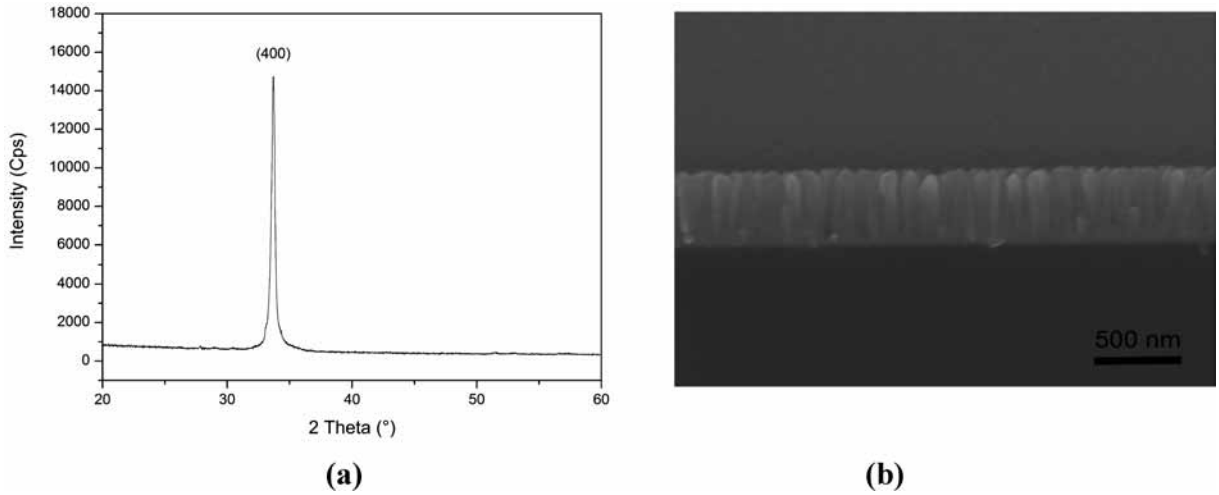

Figure 7. (a) XRD pattern and (b) cross section SEM micrograph of a Dy_2O_3 film deposited on Si(100) at 650 °C by MOCVD.

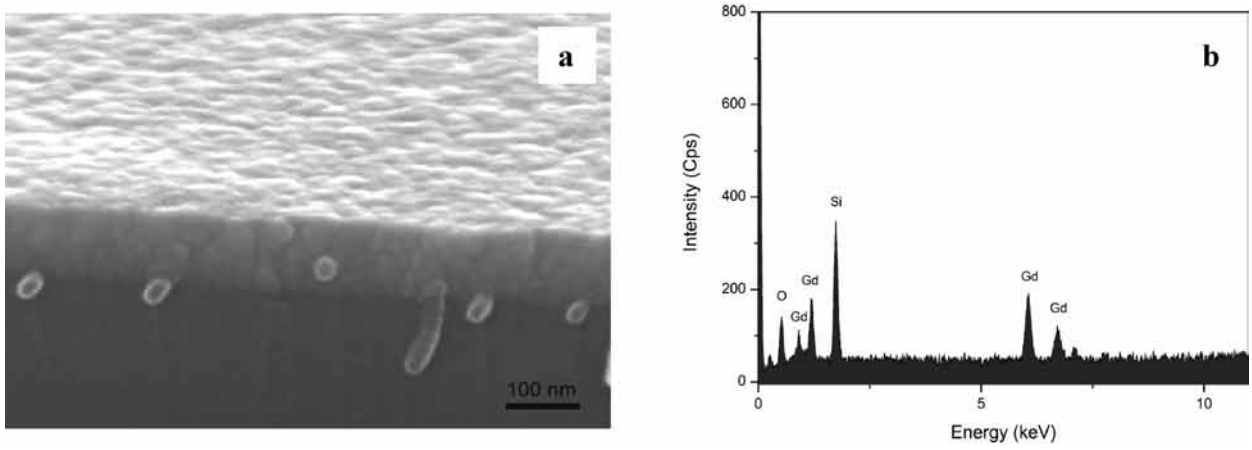

Figure 8. (a) SEM micrograph and (b) EDX spectrum of Gd_2O_3 film (ca. 100 nm) ALD deposited on Si(100) at 200 °C.

the third step in the TGA-curve at ca. 239 °C corresponds to the onset of evaporation for **2a**−**c**. This difference of 17 °C, when compared to **1a**−**c**, is most probably due to the higher molecular mass of the ^{i}Pr-Et$_2$N-guanidinates. The residual masses are higher than those observed for **1a**−**c** under the same conditions, which could be explained with partial thermal decomposition of compounds **2a**−**c** during the TGA measurement. TGA-curves of **3a**−**c**, show similar thermal behavior and comparable residual masses as those observed for **2a**−**c** (see Supporting Information, SI 5).

The thermal behavior of **1a**−**c** was further investigated using isothermal TGA-studies at four different temperatures (Table 4). At each fixed temperature, the mass loss was measured for 720 min (12 h). In all measurements, a linear weight loss was observed, which indicates that only sublimation takes place and no signs of decomposition. From the slope of the corresponding curves, the evaporation rates at different temperatures were determined. The results are plotted in Figure 5 and a linear trend for all the three complexes is observed. The evaporation rates were in the range 5.7−17.4 μg min^{-1} cm^{-2}. From the thermal studies, one can conclude that among all the rare earth complexes reported here, the Me$_2$N-Guanidinates (**1a**−**c**) show great promise for MOCVD and ALD applications.

NMR Decomposition Studies. The thermal stability of the Me$_2$N-guanidinato complexes **1a**, **c** was further investigated by NMR decomposition measurements, wherein C_6D_6 solutions of the compounds, sealed in a heavy walled NMR tubes, were heated in an oven for a long period of time. Periodically, the tubes were cooled to room temperature and ^{1}H NMR spectra were recorded. By comparing the integral areas of its NMR peaks, normalized to the solvent peak (C_6D_5H), the amount of undecomposed compound was estimated. From the linear fit of the obtained curves, the half-life of compounds **1a** and **1c** at the corresponding temperature was calculated. The decomposition studies performed at four different temperatures are summarized in Table 4 and Figure 6.

These results show that Y(^{i}Pr-Me$_2$N-guan)$_3$ **1a** and Dy(^{i}Pr-Me$_2$N-guan)$_3$ **1c** are thermally very stable compounds, which is an important requirement of an ALD precursor. For example, the half-life of **1c** at 140 °C, which is the sublimation temperature for this compound, is more than 1 year (3 months for **1a**). Even at 220 °C, which is a typical substrate temperature for ALD of rare earth oxides,[56] both compounds are remarkably stable with half-life of 125 h (**1a**)

(56) Päiväsaari, J. *Ph.D. Thesis*, Helsinki University of Technology, Espoo, 2006.

and 33.36 h (**1c**), respectively. Hence, the NMR decomposition experiments suggest that, although the surrounding environment of these precursors during an ALD process is certainly different from the one in the NMR tubes, the rare earth Me_2N-guanidinates should not thermally decompose during the short ALD cycles, when introduced in the reaction chamber.

Preliminary MOCVD and ALD Experiments. The final objective of this work was to exemplify the utility of the rare earth guanidinate complexes as precursors for the growth of rare earth oxide thin films by MOCVD and ALD. Gd(^{i}Pr-Me_2N-guan)$_3$ (**1b**) and Dy(^{i}Pr-Me_2N-guan)$_3$ (**1c**) which showed the most promising properties in terms of volatility and thermal stability were selected for film deposition. MOCVD of Dy_2O_3 was performed using Dy(^{i}Pr-Me_2N-guan)$_3$ (**1c**) and using oxygen as the oxidant. The growth rates of Dy_2O_3 thin films were of the order of 7−16 nm/min. From the XRD measurements, polycrystalline films were grown at lower temperatures (400−550 °C). When the substrate temperature was increased beyond 600 °C, highly oriented cubic Dy_2O_3 were obtained. The diffractogram shown in Figure 7a shows that the Dy_2O_3 film grown at 650 °C from compound **1c** is highly oriented in the (400) direction [fwhm = 0.317°, 33.58° (2θ)]. The film morphology investigated by SEM revealed the formation of columnar and oriented grains as seen in Figure 7b for a Dy_2O_3 film deposited at 650 °C.

ALD of Gd_2O_3 was attempted in the temperature range between 200 − 350 °C using Gd(^{i}Pr-Me_2N-guan)$_3$ (**1b**) in combination with water as the oxidant. Growth rates up to 1 Å per cycle were obtained under the adopted ALD conditions. The as-grown films at 200 °C appeared to be amorphous according to XRD measurements and the amorphous nature of the films was also seen from the SEM surface morphology (see Figure 8a). The composition of the films was measured by EDX analysis and the presence of Gd and O in the films was confirmed (see Figure 8b). At this point, detailed ALD studies are required in order to determine whether a self-limiting ALD-type growth occurs throughout the given temperature range. The detailed studies on the MOCVD and ALD of Dy_2O_3 and Gd_2O_3 are currently underway and will be published separately.

Conclusions

With the use of guanidinates as chelating ligands, a series of novel homoleptic rare-earth complexes of Y, Gd and Dy have been developed. All the compounds are monomeric and volatile showing clean sublimation behavior. NMR decomposition studies revealed the extraordinary thermal stability of these compounds at temperatures as high as the evaporation and deposition temperature during ALD. Given the limited choice of precursors available for MOCVD and ALD of rare-earth oxide thin films, the isopropyl amido-guanidinato complexes of Y, Gd and Dy reported here are highly promising precursors both for MOCVD and ALD. Our work presented here concerns precursor development and characterization. Further studies will be devoted to detailed thin film growth and characterization of rare-earth oxides by MOCVD and ALD and to eventually investigate the functional properties of these oxides. In particular, the growth of Gd_2O_3 will be optimized in view of their potential use as high-k gate oxide material for metal-oxide-semiconductor (MOS) capacitors, as they are projected to be excellent candidates for replacing SiO_2 as the gate oxide material.

Acknowledgment. Financial support from the German Science Foundation (DFG, CVD-SPP-1119, DE-790/3-3) is gratefully acknowledged. The authors thank Prof. W. Sheldrick, M. Winter and Dr. H. Parala for their help in X-ray anaylsis. Dr. R. Pothiraja, Dr. H. Parala and Dr. G. Prabusankar are acknowledged for helpful discussions and for the critical comments on the manuscript.

Supporting Information Available: ^{1}H NMR spectrum of **1a** (250 MHz, RT, C_6D_6); overview of the fragments of complexes **2a**−**c** and **3a**,**b** observed in the mass spectra; TGA plots of rare earth guanidinato complexes **2a**−**c** and **3a**−**c**; physical data of rare earth guanidinato complexes **2a**−**c**, **3a**−**c**; XRD pattern of Gd_2O_3 film deposited on Si(100) at 650 °C by MOCVD (fwhm = 0.251°@33.115 (2θ)); the molecular structure of Dy[(N^{i}Pr)$_2$CNMe$_2$]$_3$ (**1c**) in the solid state. The two planes N1N5N7 and N2N3N8 are highlighted. This material is available free of charge via the Internet at http://pubs.acs.org.

IC801432B